Determination of the Secondary Structure of the DNA Binding Protein Ner from Phage Mu Using ^{1}H Homonuclear and ^{15}N–^{1}H Heteronuclear NMR Spectroscopy[†]

Angela M. Gronenborn,*[,‡] Paul T. Wingfield,[§] and G. Marius Clore*[,‡]

Laboratory of Chemical Physics, National Institute of Diabetes and Digestive and Kidney Diseases, National Institutes of Health, Bethesda, Maryland 20892, and Glaxo Institute for Molecular Biology SA, 46 Route des Acacias, CH 1211 Geneva, Switzerland

Received December 29, 1988; Revised Manuscript Received March 6, 1989

ABSTRACT: The sequential resonance assignment of the ^{1}H and ^{15}N NMR spectra of the DNA binding protein Ner from phage Mu is presented. This is carried out by using a combination of ^{1}H–^{1}H and ^{1}H–^{15}N two-dimensional experiments. The availability of completely labeled ^{15}N protein enabled us to record a variety of relayed heteronuclear multiple quantum coherence experiments, thereby enabling the correlation of proton–proton through-space and through-bond connectivities with the chemical shift of the directly bonded ^{15}N atom. These heteronuclear experiments were crucial for the sequential assignment as the proton chemical shift dispersion of the Ner protein is limited and substantial overlap precluded unambiguous assignment of the homonuclear spectra in several cases. From a qualitative interpretation of the NOE data involving the NH, C$^\alpha$H, and C$^\beta$H protons, it is shown that Ner is composed of five helices extending from residues 11 to 22, 27 to 34, 38 to 45, 50 to 60, and 63 to 73.

The Ner protein of bacteriophage Mu plays a crucial role in the switch between lytic and lysogenic development of the phage, exerting its function at the transcriptional level (van de Putte et al., 1980). Ner negatively regulates early transcription, thereby autoregulating its own expression as well as inhibiting expression of the C repressor gene (van Leerdam et al., 1980). The target sequences on the DNA have been identified by genetic mapping (Goosen, 1984; Goosen & van de Putte, 1984) and footprinting (Tolias & DuBow, 1986). These comprise two tandem repeats of a dodecanucleotide interrupted by a six nucleotide spacer. The Ner binding sites overlap the early promoter (Pe) as well as the repressor promoter (Pc-2).

Despite the functional similarities between the cro protein of λ and the Ner protein of Mu, no obvious homologies are apparent at the amino acid level. It is therefore not clear if the homology found for a large number of DNA binding proteins in the region of supersecondary structure involved in sequence-specific DNA recognition, the so-called helix–turn–helix motif (Anderson et al., 1982; Pabo & Sauer, 1984), is also present in the Ner protein. To date, nothing is known about either the secondary or tertiary structure of Ner, and there are no preliminary crystallographic reports in the literature on this protein. We therefore decided to embark on a nuclear magnetic resonance (NMR)[1] study of the Ner protein in solution with the aim of determining its three-dimensional structure.

We recently described the construction of an expression system that directs high-level synthesis of the *ner* gene product in *Escherichia coli* as well as the large-scale purification and characterization of the 75 amino acid containing Ner protein (Allet et al., 1988) aimed at providing enough purified protein for our work.

In this paper we describe the use of a combination of two-dimensional ^{1}H homonuclear and ^{15}N–^{1}H heteronuclear experiments to sequentially assign both the ^{1}H and ^{15}N NMR spectrum of Ner and to delineate its secondary structure.

MATERIALS AND METHODS

Sample Preparation. Ner protein was purified from *E. coli* B harboring the expression plasmid pL-ner that contains the *ner* gene behind an inducible λ promoter as described previously (Allet et al., 1988). Samples for NMR were dialyzed against 20–30 mM sodium phosphate buffer, pH 7.0, freeze-dried, and subsequently dissolved at a concentration of 2–3 mM protein. The final buffer concentration was 100–150 mM sodium phosphate in either 99.96% D_2O or 90% H_2O/10% D_2O. The pH of the samples was adjusted with small amounts of DCl.

The uniformly ^{15}N labeled sample was prepared from bacteria grown in minimal medium using ^{15}NH$_4$Cl as the sole nitrogen source.

NMR Spectroscopy. NMR measurements were carried out at 600 MHz on a Bruker AM-600 spectrometer equipped with digital phase shifters, a "reverse" mode ^{1}H probe, and an Aspect 3000 computer. All two-dimensional spectra were recorded in the pure phase absorption mode by using the time proportional incrementation method (Redfield & Kunz, 1975) as described by Marion and Wüthrich (1983). NOESY spectra (Jeener et al., 1979; Macura et al., 1981) with mixing times of 100 and 200 ms and HOHAHA spectra (Braunschweiler & Ernst, 1983; Davis & Bax, 1985) with a WALTZ17 mixing sequence (Bax, 1989) of 30–60 ms sandwiched between 1.5-ms trim pulses were recorded at 27 and 36 °C and at several different pHs. ^{15}N–^{1}H HMQC spectra (Mueller, 1979; Redfield, 1983; Bax et al., 1983; Sklenar &

[1] Abbreviations: NMR, nuclear magnetic resonance; NOE, nuclear Overhauser effect; NOESY, two-dimensional nuclear Overhauser enhancement spectroscopy; DQF-COSY, two-dimensional double quantum filtered correlated spectroscopy; P-COSY, two-dimensional primitive correlated spectroscopy; PS-COSY, two-dimensional pseudo single quantum correlated spectroscopy; HOHAHA, two-dimensional homonuclear Hartmann–Hahn spectroscopy; HMQC, two-dimensional heteronuclear multiple quantum correlated spectroscopy; HMBC, two-dimensional heteronuclear multiple bond correlation spectroscopy.

Bax, 1987; Glushka & Cowburn, 1987), HMQC–NOESY spectra (Gronenborn et al., 1989) and HMQC–COSY spectra (Clore et al., 1988) were also recorded at several temperatures and pHs. The PS-COSY, P-COSY, and HMBC experiments were recorded as described by Bax et al. (1989), Marion and Bax (1988a), and Bax and Marion (1988), respectively.

For NOESY spectra recorded in H_2O, the water resonance was suppressed by using a semiselective "jump-return" pulse (Plateau & Gueron, 1982) in place of the last 90° pulse in the NOESY sequence. Water suppression in the HOHAHA spectra was achieved by using a 90° "flip-back" pulse, a 100-μs recovery delay, and the jump-return sequence after the WALTZ17 mixing sequence (Bax et al., 1987). The effects of radiation damping were minimized by cycling the phase of the preparation pulse 45° out of register with those of the evolution and detection periods (Driscoll et al., 1989). Optimization of the receiver phase to eliminate base-line distortions was carried out according to the method of Marion and Bax (1988b), and suppression of t_2 ridges was achieved by zeroing the first point of each FID as well as linear base-line corrections of both the initial FIDs prior to Fourier transformation in F_2 and the F_2 cross sections prior to Fourier transformation in F_1 (Driscoll et al., 1989).

Typically, 800–1024 increments of 2K data points were collected for each NOESY and HOHAHA experiment resulting in 2D spectra with a digital resolution of the order of 6–8 Hz/point in each dimension after zero-filling. In the case of the P-COSY and PS-COSY experiments 1024 increments of 4K data points were collected, and the digital resolution in F_2 was 1.7 Hz/point.

For the P-COSY experiment, a reference one-dimensional FID was recorded with a 0° mixing pulse, $t_1 = 0$ μs, and 128 scans, 8 times the number of scans used per increment in the COSY experiment recorded with a 70° mixing pulse. By left shifting the data of this single reference FID, we obtained the time domain data for successive values of the 0° COSY experiment. The 0° COSY time domain data were then subtracted from the 70° COSY time domain data to generate the P-COSY time domain data. By this means the dispersive character of the diagonal in a regular COSY spectrum is purged, and the sensitivity of the resulting spectrum is approximately twice that of a conventional DQF-COSY spectrum recorded in the same measuring time (Marion & Bax, 1988a).

The ^{15}N–^1H HMQC, ^{15}N–^1H HMQC–NOESY, and ^{15}N–^1H HMQC–COSY spectra were recorded with spectral widths of 10 000 and 4166.6 Hz in the ^1H and ^{15}N dimensions, respectively. Eight hundred increments were collected for each spectrum with 16 and 32 scans per t_1 value for the correlation and relayed correlation experiments, respectively. Water suppression was achieved by presaturation during the relaxation delay and, in the case of the ^{15}N–^1H HMQC–NOESY experiment, during the mixing time as well. The digital resolution for the HMQC and HMQC–NOESY spectra was 4.1 Hz/point in F_1 and 4.9 Hz/point in F_2, the latter being obtained by appropriate zero-filling. For the HMQC–COSY spectra, the digital resolution in F_2 was 2.4 Hz/point.

For the ^{15}N–^1H HMBC experiment 512 increments of 1K data points were collected for spectral widths of 4310 and 5494 Hz in the ^{15}N and ^1H dimensions, respectively. The final digital resolution after appropriate zero-filling was 4.2 and 5.4 Hz/point in the ^{15}N and ^1H dimensions, respectively.

RESULTS AND DISCUSSION

The sequential assignment of the Ner protein spectrum was carried out by identifying through-bond scalar and through-space connectivities (Billeter et al., 1982; Wüthrich, 1986). In contrast to the procedures generally used to date, which have relied entirely on ^1H homonuclear experiments, we have made use of a combination of homonuclear and ^{15}N–^1H heteronuclear experiments. The availability of the completely ^{15}N labeled protein, which allowed us to record a variety of HMQC-relayed spectra, was of crucial importance for the assignment as the proton chemical shift dispersion of the Ner protein is limited and substantial overlap precluded unambiguous assignment of the homonuclear spectra in several cases. In addition, the protein is only stable over a pH range between 5 and 7, undergoing major conformational changes (unfolding) at pH values below 4 and an as yet unidentified conformational change around pH 7.8. Similarly, the allowed temperature range is fairly narrow, being limited to values below 40 °C.

Amino acid spin systems were identified by using P-COSY, PS-COSY, HOHAHA, HMQC, and relayed ^1H–^{15}N HMQC–COSY spectra, while through-space connectivities were established by means of NOESY and relayed ^1H–^{15}N HMQC–NOESY spectra.

It is worth pointing out two amino acids exhibiting extremely high field shifts, namely, Gly-50 ($C^\alpha H$, 2.73 and 2.20 ppm) and Ile-65 ($C^\alpha H$, 1.87; $C^\beta H$, 0.30 ppm). These resonance positions are about 1.7 ppm (Gly-50 $C^\alpha Hs$) and 2.5 ppm (Ile-65 $C^\alpha H$) upfield of the respective random coil position, most likely due to close spacial proximity of aromatic rings. By comparing the HOHAHA spectra, recorded at several different mixing times between 17 and 60 ms, with the P-COSY spectrum (not shown) direct, single, and multiple relayed connectivities could easily be distinguished. The aliphatic region of a HOHAHA spectrum in D_2O is included as supplementary material.

Figure 1A shows the so-called fingerprint region (NH–$C^\alpha H$ region) of a through-bond correlated spectrum recorded with ^{15}N filtering. In the conventional ^1H–^1H DQF-COSY spectrum of the Ner protein less than 50% of the expected cross peaks were visible (spectrum not shown), principally due to the small size of $^3J_{HN\alpha}$ couplings relative to the amide proton line widths. In the ^{15}N-filtered pseudo single quantum COSY (PS-COSY; Bax et al., 1989) recorded on the uniformly ^{15}N labeled sample shown in Figure 1A, most NH–$C^\alpha H$ cross peaks can be observed. This improvement is due to the fact that one of the major line-broadening mechanisms for amide protons in proteins, namely, heteronuclear coupling to the nitrogen nucleus (Ernst et al., 1987), is removed by generating heteronuclear zero and double quantum coherences whose relaxation rates, to a first-order approximation, are not affected by heteronuclear dipolar coupling. The ^{15}N chemical shift contribution is easily removed from the multiple quantum frequency, yielding a spectrum that has the same general appearance as a regular COSY or DQF-COSY spectrum except that the lines of the NH resonances are narrowed. The missing cross peaks are due to presaturation of the water resonance, which prevents the detection of fast-exchanging resonances and resonances whose $C^\alpha H$ chemical shifts lie under the water resonance. Unfortunately, this cannot be avoided as the heteronuclear zero and double quantum coherences have to be present during the t_1 evolution period so that the $C^\alpha H$ resonances have to be detected during t_2.

Complementing the traditional fingerprint region of the PS-COSY spectrum is the relayed ^{15}N–^1H HMQC–COSY spectrum that exhibits NH–$C^\alpha H$ cross peaks spread out according to the ^{15}N chemical shifts of the amide resonances in contrast to the conventional proton chemical shifts. The ^{15}N
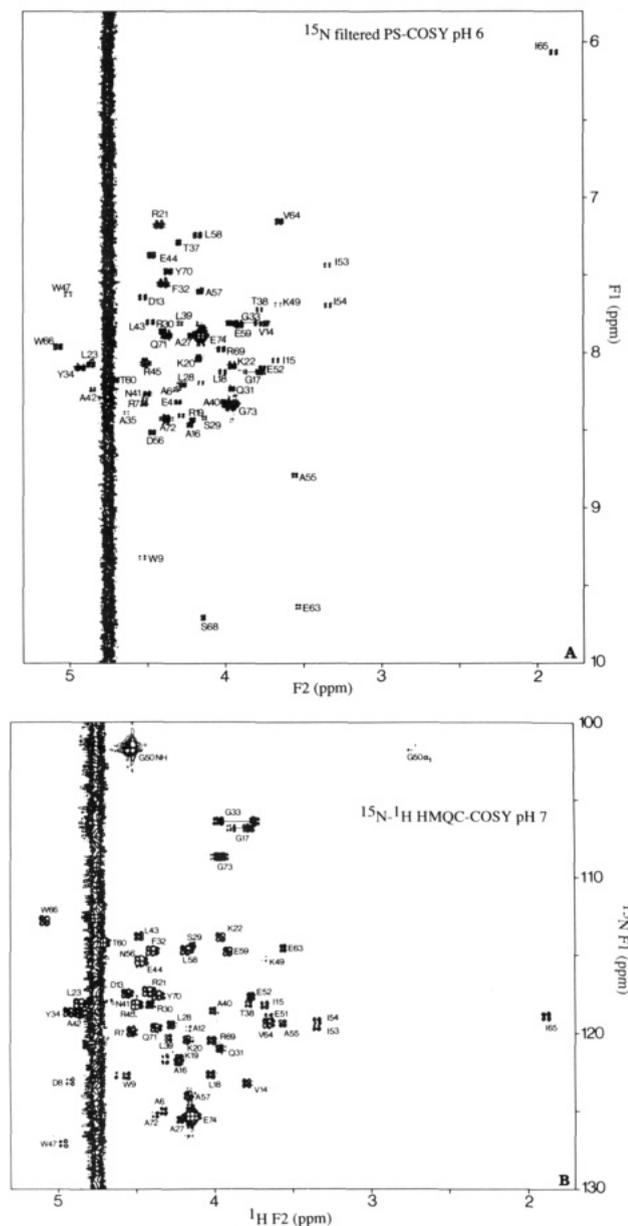
FIGURE 1: (A) NH(F_1 axis)–C$^\alpha$H(F_2 axis) region of the ^{15}N-filtered PS-COSY spectrum of the uniformly ^{15}N labeled Ner protein in H$_2$O at 27 °C and pH 6.0. (B) ^{15}N (F_1 axis)–C$^\alpha$H(F_2 axis) region of the ^{15}N–^{1}H HMQC–COSY spectrum of the uniformly labeled ^{15}N Ner protein in H$_2$O at 27 °C and pH 7.0. Cross peaks in (B) arise from C$^\alpha$H(i)–^{15}N(i) connectivities via an indirect pathway involving two successive one-bond scalar couplings, namely, ^{15}N(i)–NH(i) and NH(i)–C$^\alpha$H(i).

aliphatic region of this spectrum is shown in Figure 1B. (As in the case of the PS-COSY spectrum, suppression of the water resonance by presaturation cannot be avoided.) A comparison of the two spectra clearly documents that the spread of NH–C$^\alpha$H cross peaks according to the NH proton chemical shifts (Figure 1A) is quite different from that according to the ^{15}N chemical shift (Figure 1B). For example, the Trp-47 cross peak is located at the upper left in the PS-COSY spectrum, while it is found in the lower left in the HMQC–COSY one, thus allowing one to extract complementary information from the HMQC–COSY spectrum.

The ^{15}N–^{1}H HMQC spectrum of the Ner protein at pH 7 is shown in Figure 2A. Of the potential 69 ^{15}N–^{1}H amide correlation cross peaks, 61 are present in the spectrum, those missing belonging to amide protons that undergo rapid exchange with water. (The HMQC spectrum was also recorded

with presaturation of the water resonance.) Of interest is the very high field shifted NH resonance of Gly-50 (4.5 ppm) that is correlated with the high-field chemical shifts of its C$^\alpha$H resonances (cf. Table I). In addition, correlation cross peaks for the NH$_2$ groups of asparagines and glutamines can be observed as well as for tryptophan indole amide protons. The glycine correlation peaks are found at the high-field end of the amide ^{15}N chemical shift axis and are easily identified in conjunction with the ^{1}H–^{15}N HMQC–COSY spectrum (Figure 1B), thereby providing useful starting points for sequential connectivities in the ^{1}H–^{15}N HMQC–NOESY spectra.

NOESY spectra were employed to observe through-space (<5 Å) connectivities. For the purposes of sequential assignment, the NOEs involving NH, C$^\alpha$H, and C$^\beta$H protons are the most useful. In addition to the usual ^{1}H–^{1}H NOESY spectra, much emphasis was also placed on ^{15}N–^{1}H HMQC–NOESY spectra.

Figure 3 shows the NH–NH region of two NOESY spectra. In the spectrum at pH 7 (Figure 3A) NH(i)–NH(i + 1) connectivities extending from residue 51 to residue 60 and from residue 63 to residue 66 are indicated, while in the pH 5 spectrum (Figure 3B) connectivities from residue 9 to residue 17 and from residue 24 to residue 33 are shown. In the pH 7 spectrum, NH–NH and C$^\alpha$H–NH connectivities involving the NH protons of Arg-11, Leu-25, and Ser-26 are absent, while they are clearly visible in the pH 5 spectrum. This must reflect high exchange rates for these amide protons, resulting in extensive line broadening, as the spectra were recorded without perturbing the water magnetization. The structural features of these regions, however, are probably very similar at the two pH values as bridging NH–NH NOEs between His-10 and Ala-12, Ser-24 and Ala-27, and Ser-24 and Leu-28 (Figure 3A,B) as well as the NOEs between the C$^\alpha$H and C$^\beta$H protons of His-10 and the NH proton of Ala-12 are present in both spectra.

Complementing the NH–NH region of the NOESY spectrum is the NH(F2)–aliphatic(F1) region shown in Figure 4 for the pH 5 data. Numerous C$^\alpha$H(i)–NH(i + 1) and C$^\beta$H-(i)–NH(i + 1) NOE connectivities, as well as some C$^\alpha$H-(i)–NH(i + 2,3) connectivities, are indicated that confirm the NH(i)–NH(i + 1) connectivities shown in Figure 3. Thus, for example, stretches of connectivities extending over residues 8–17, 23–27, and 55–60 are illustrated. This region of the NOESY spectrum at pH 7 is given in the supplementary material.

NH–NH NOESY connectivities in the ^{1}H–^{15}N HMQC–NOESY spectrum are illustrated in Figure 2B. Several consecutive stretches are indicated, namely, over residues 12–17, 18–23, 27–34, 55–58, and 63–66. Obviously, the NH–NH connectivities are the same as those observed in a conventional NOESY spectrum (Figure 3). The absence of a diagonal together with the fact that ^{15}N chemical shifts are in general not correlated with ^{1}H ones makes it possible to detect NOEs between NH protons with only slightly different proton chemical shifts. As a further demonstration of the usefulness of the ^{15}N–^{1}H HMQC–NOESY spectra we describe the case of Gly-17 and Leu-18. Since the amide resonances of Gly-17 and Leu-18 are degenerate, one cannot observe an NOE between them in the NH region of the spectrum at pH 7. Inspection, however, of the aliphatic region of this spectrum (Figure 2C) clearly shows C$^\alpha$H(i)–NH(i + 1) connectivities along the stretch comprising residues 13–23, including the connectivity between Gly-17 and Leu-18. This connection cannot be observed in the conventional ^{1}H–^{1}H

FIGURE 2: ^{15}N–^{1}H HMQC and ^{15}N–^{1}H HMQC–NOESY spectra of the uniformly labeled Ner protein in H$_2$O at 27 °C and pH 7.0. (A) ^{15}N(F_1 axis)–NH(F_2 axis) region of the HMQC spectrum. (B) ^{15}N(F_1 axis)–NH(F_2 axis) region and (C) ^{15}N(F_1 axis)–aliphatic(F_2 axis) region of the relayed ^{15}N–^{1}H HMQC–NOESY (200 ms) spectrum. The cross peaks in (A) and (B) are labeled at the position of the intraresidue ^{15}N(i)–NH(i) connectivity, while those in (C) are labeled at the position of the ^{15}N(i)–C$^{\alpha}$H(i) or ^{15}N(i)–C$^{\beta}$H(i) connectivity (indicated by β). A number of sequential NH(i)–NH(i + 1) connectivities are indicated in (B), while sequential C$^{\alpha}$H(i)–NH(i + 1) and C$^{\beta}$H(i)–NH(i + 1) NOE connectivities are indicated by continuous lines in (C). Some other types of NOE connectivities are indicated in (C) by dashed lines.
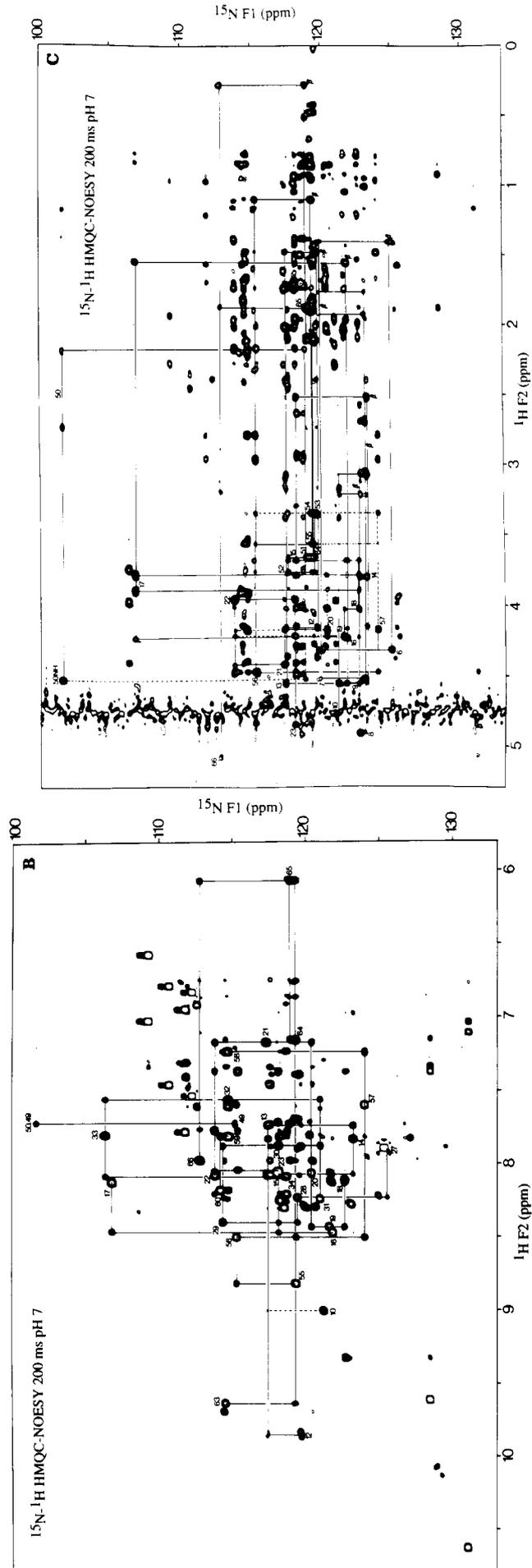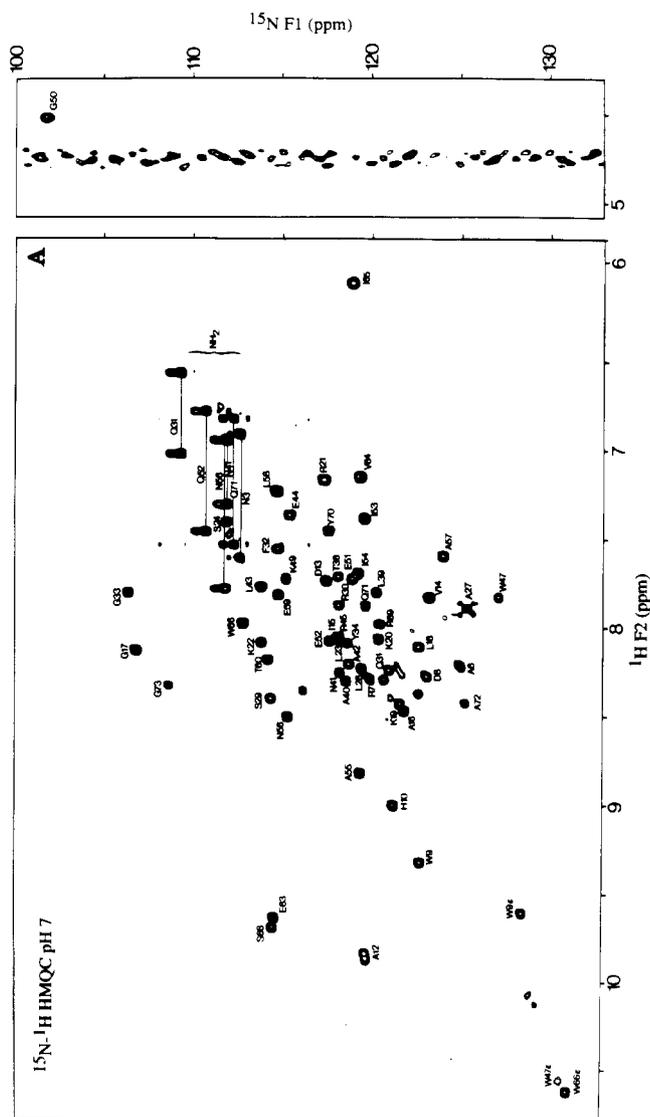
Table I: ^{15}N and ^{1}H Chemical Shifts (ppm) of Mu Ner at 27 °C and pH 7.0[a]

residue	^{15}N	NH	C$^{\alpha}$H	C$^{\beta}$H	others
A6	125.0	8.22	4.22	1.40	
R7	119.9	8.28	4.53	1.83, 1.83	
D8	123.2	8.28	4.92	2.97, 2.69	
W9	122.8	9.32	4.56	3.24, 3.09	C$^{\delta 1}$H 7.38; C$^{\zeta 2}$H 7.34; C$^{\eta}$H 7.15;
	N$^{\epsilon}$ 128.5				C$^{\zeta 3}$H 6.83; C$^{\epsilon 3}$H 6.89; N$^{\epsilon}$H 9.60
H10	121.3	9.00	4.8[b]	3.37, 3.17	C$^{\epsilon 1}$H 8.08; C$^{\delta 2}$H 7.30
					pK $\sim$ 7.5[c]
R11	126.3[d]	9.59[d]	4.15		
A12	119.8	9.85	4.17	1.48	
D13	117.5	7.74	4.56	3.09, 2.60	
V14	123.2	7.83	3.79	2.54	C$^{\gamma}$H$_3$ 1.02, 0.96
I15	118.2	8.07	3.67	1.97	C$^{\gamma 2}$H$_3$ 1.06
A16	121.8	8.48	4.23	1.55	
G17	106.8	8.13	3.88, 3.77		
L18	122.6	8.12	4.03		
K19	121.7	8.44	4.01		
K20	120.4	8.07	4.17		
R21	117.3	7.18	4.42		
K22	113.9	8.09	3.96		
L23	118.0	8.07	4.86	1.73	C$^{\gamma}$H 1.24; C$^{\delta}$H 1.00
S24	111.9	7.41	4.7[b]	4.27, 3.94	
L25	124.0[d]	9.60[d]	4.00		
S26	114.8[d]	8.55[d]	3.88	3.95	
A27	125.5	7.89	4.21	1.57	
L28	119.5	8.24	4.27		
S29	114.4	8.41	4.14	4.25, 4.15	
R30	118.2	7.88	4.41		
Q31	121.0	8.24	4.26	2.30, 2.16	N$^{\epsilon}$H$_2$ 7.03, 6.58
	N$^{\epsilon}$ 109.3				
F32	114.8	7.57	4.40	3.43, 2.80	C$^{\delta}$H 7.63; C$^{\epsilon}$H 7.35; C$^{\zeta}$H 7.31
G33	106.4	7.81	3.97, 3.74		
Y34	118.7	8.09	4.93	3.34, 2.98	C$^{\delta}$H 7.25; C$^{\epsilon}$H 6.87
A35	119.6	8.38	4.62	1.57	
P36					C$^{\delta}$H 3.96, 3.89; C$^{\gamma}$H 1.53
T37	102.5[d]	7.31[d]	4.28	4.46	
T38	118.2	7.72	3.78	4.02	
L39	120.3	7.80	4.29	1.78, 1.69	C$^{\gamma}$H 1.47
A40	118.6	8.30	4.01	1.51	
N41	118.2	8.25	4.51	2.94, 2.63	N$^{\delta}$H$_2$ 7.11, 6.96
	N$^{\delta}$ 111.8				
A42	118.8	8.20	4.85	1.38	
L43	113.8	7.77	4.48	2.18	C$^{\gamma}$H 1.98; C$^{\delta}$H 1.12, 1.18
E44	115.4	7.37	4.45	2.18, 2.02	C$^{\gamma}$H 2.33, 2.27
R45	118.2	8.05	4.48	1.75, 1.65	C$^{\gamma}$H 1.56, 1.37; C$^{\delta}$H 3.08
H46	121.7	8.36	4.60	3.22, 2.78	C$^{\epsilon 1}$H 7.68; C$^{\delta 2}$H 7.12
					pK = 6.45
W47	127.1	7.82	4.96	3.30, 3.10	C$^{\delta 1}$H 7.24; C$^{\zeta 2}$H 7.29
	N$^{\epsilon}$ 130.7				C$^{\eta}$H 6.93; C$^{\zeta 3}$H 6.73; C$^{\epsilon 3}$H 7.25; N$^{\epsilon}$H 10.57
P48					C$^{\delta 1}$H 3.64; C$^{\delta 2}$H 2.46
K49	115.2	7.73	3.67	1.69, 1.19	
G50	101.7	4.53	2.73, 2.20		
E51	118.9	7.73	3.65	2.10	C$^{\gamma}$H 2.42, 1.22
Q52	117.6	8.06	3.76	2.11, 2.04	C$^{\gamma}$H 2.47, 2.37
	N$^{\epsilon}$ 110.7				N$^{\epsilon}$H$_2$ 7.47, 6.80
I53	119.6	7.39	3.34	1.55	C$^{\gamma 2}$H$_3$ 0.81; C$^{\delta}$H$_3$ 0.02
I54	119.2	7.70	3.35	1.91	C$^{\gamma 2}$H$_3$ 0.49; C$^{\delta}$H$_3$ 0.66
A55	119.3	8.82	3.56	1.10	
N56	115.3	8.51	4.47	2.97, 2.79	N$^{\delta}$H2 7.79, 6.94
	N$^{\delta}$ 111.8				
A57	124.0	7.60	4.16	1.58	
L58	114.7	7.24	4.18		
E59	114.8	7.82	3.91	2.22	
T60	114.2	8.18	4.69	3.87	C$^{\gamma 2}$H$_3$ 0.86
K61		8.30	4.81	3.94	
P62					C$^{\delta 1}$H 3.86; C$^{\delta 2}$H 3.70
E63	114.6	9.63	3.55		
V64	119.4	7.17	3.66	2.13	C$^{\gamma 1}$H$_3$ 0.93; C$^{\gamma 2}$H$_3$ 0.87
I65	118.9	6.07	1.87	0.30	C$^{\gamma 1}$H$_2$ -1.79; C$^{\gamma 2}$H$_3$ -1.57; C$^{\delta}$H$_3$ -0.35
W66	112.8	7.98	5.08	3.20, 2.89	C$^{\delta 1}$H 7.11; C$^{\zeta 2}$H 7.03; C$^{\eta}$H 6.77;
	N$^{\epsilon}$ 131.1				C$^{\zeta 3}$H 6.88; C$^{\epsilon}$H 7.79; N$^{\epsilon}$H 10.63
P67					C$^{\delta 1}$H 3.81; C$^{\delta 2}$H 3.13; C$^{\gamma}$H 4.92
S68	114.5	9.69	4.10	3.90	
R69	120.5	7.98	4.02		
Y70	117.6	7.47	4.37	3.35, 2.44	C$^{\delta}$H 7.36; C$^{\epsilon}$H 6.77
Q71	119.7	7.88	4.38	2.15, 2.02	C$^{\gamma}$H 2.39
	N$^{\epsilon}$ 112.3				N$^{\epsilon}$H$_2$ 7.54, 6.84
A72	125.2	8.43	4.38	1.41	
G73	108.7[d]	8.35[d]	3.99, 3.93		
E74	125.3	7.90	4.15		

[a] ^{1}H chemical shifts are expressed relative to 4,4-dimethyl-4-silapentane-1-sulfonate, ^{15}N ones relative to external liquid NH$_3$. [b] Resonance lies under the water resonance. [c] Discontinuity in the titration curve between pH 7.8 and 8.2. [d] Resonance is not visible in the pH 7.0 spectrum; the values given are for the pH 5.0 spectrum.
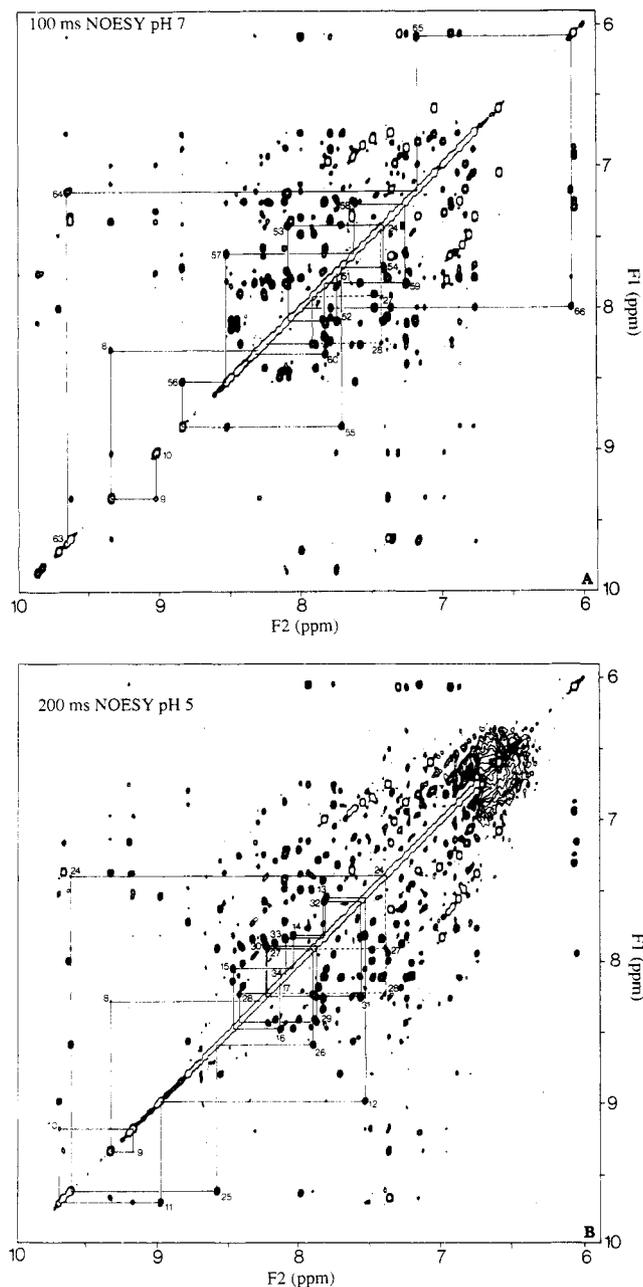
FIGURE 3: (A) NH(F_1 axis)–NH(F_2 axis) region of the 100-ms NOESY spectrum of Ner in H_2O at 27 °C and pH 7.0. (B) NH(F_1 axis)–NH(F_2 axis) region of the 200-ms NOESY spectrum of Ner in H_2O at 27 °C and pH 5.0. The sequential NH(i)–NH(i + 1) NOE connectivities extending over residues 8–10, 51–60, and 63–66 (A) and 8–17 and 24–34 (B) are indicated by continuous lines, while NH(i)–NH(i + 3,4) connectivites involving residues 24, 27, and 28 are marked by a dashed line.

NOESY spectrum, since in this case the $C^\alpha H$ proton resonances are spread out according to their amide proton chemical shifts, which for residues 17 and 18 are identical. Several situations of this kind could be dealt with satisfactorily by using the relayed ^{15}N–^1H HMQC–NOESY spectra. Also of interest is the stretch of NH(i)–NH(i + 1) connectivities from residue 49 to residue 51. It was very difficult to establish NH(i)–NH(i + 1) connectivities involving Gly-50 from the conventional NOESY spectrum as its NH resonance has such an unusual chemical shift and is very close to the water resonance. These connectivities are easily apparent, however, in the ^{15}N–^1H HMQC–NOESY spectrum (Figure 2B,C).

Figure 5 shows part of the ^1H-detected ^{15}N multiple bond correlation (HMBC) spectrum in which multiple bond scalar

connectivities between ^{15}N and $C^\alpha H$ atoms can be observed. Using the HMQC–COSY spectrum (Figure 1B) to locate the intraresidue $^{15}N(i)$–$C^\alpha H(i)$ cross peaks, it is possible to sequentially walk along the polypeptide backbone via two-bond $^{15}N(i)$–$C^\alpha H(i)$ and three-bond $C^\alpha H(i)$–$^{15}N(i + 1)$ scalar connectivities in contrast to the through-space connectivities employed in the traditional sequential assignment strategy based on NOESY spectra. This works particularly well for helical and turn regions, since relatively large (4–6 Hz) three-bond $C^\alpha H(i)$–$^{15}N(i + 1)$ coupling constants are expected for ψ backbone torsion angles in the range –40° to –80° characteristic of α-helices and type I turns (Bystrov, 1976). All long-range (three-bond) connectivities identified in this manner are shown in the first line of the sequential connectivity diagram of Figure 6. The combination of the HMBC and the HMQC–COSY spectra was extremely useful for the sequential assignment providing confirmation for a variety of NOESY connectivities throughout the entire sequence.

From the analysis of all spectra described above, supplemented by information from spectra at different temperatures and pH values, it was possible to arrive at almost complete assignments for the ^{15}N, amide proton, and $C^\alpha H$ proton resonances. A summary of the assignments to date is given in Table I, and the complete set of connectivities determined from both the homonuclear and heteronuclear spectra is summarized with the amino acid sequence in Figure 6. No unambiguous assignments could be obtained for the first five amino acids due to the absence of convincing connectivities as well as the occurrence of multiple conformations in this region.

Qualitative interpretation (Wüthrich et al., 1984) of the short-range NOEs involving the NH, $C^\alpha H$, and $C^\beta H$ protons summarized in Figure 6 allows one to delineate the secondary structure of the Ner protein. It basically consists of five α-helices, as evidenced by stretches of strong NH(i)–NH(i + 1) connectivities in conjunction with diagnostic $C^\alpha H(i)$–NH(i + 3), NH(i)–NH(i + 2), and $C^\alpha H(i)$–NH(i + 2) NOEs. The helical regions extend over residues 11–22, 27–34, 38–45, 50–60, and 63–73 and are schematically indicated at the bottom of Figure 6. For the first and fourth helices a number of $C^\alpha H(i)$–$C^\beta H(i + 3)$ as well as $C^\alpha H(i)$–NH($i + 4$) connectivities are observed, providing additional support for the α-helical structure. For the third and fifth helices only a few $C^\alpha H(i)$–NH(i + 3) connectivites were observed, but since all other sequential NOEs support a helical conformation, we believe that indeed those stretches are α-helices. Additional evidence can be derived from the three-bond $C^\alpha H(i)$–$^{15}N(i + 1)$ correlations found in the HMBC spectrum, which also support a helical structure. At the present stage, however, it is not clear where the exact start and end of the helices is located, since turns located at the start or end of a helix are difficult to distinguish from the helix itself on the basis of sequential NOEs alone. For instance, considering the first helix, we observe weak sequential NH(i)–NH(i + 1) connectivities at pH 5 from residues 8–11 followed by strong ones from residue 11 upward (Figure 3B). At pH 7 we observe a stretch of medium-strength NH(i)–NH(i + 1) NOEs from residues 8–10 (Figure 3A), followed by strong ones from residue 12 upward. At pH 7, however, we cannot observe the NH resonance of Arg-11 due to fast exchange with water, suggesting that the NH of Arg-11 is not hydrogen-bonded. If the first helix would actually start at Asp-8, the first hydrogen-bonded amide would belong to Ala-12. Interestingly, this is exactly the amide proton resonance that exhibits a large pH dependence of its chemical shift, moving downfield by 0.9 ppm as the pH is increased from 5 to 7. A somewhat smaller
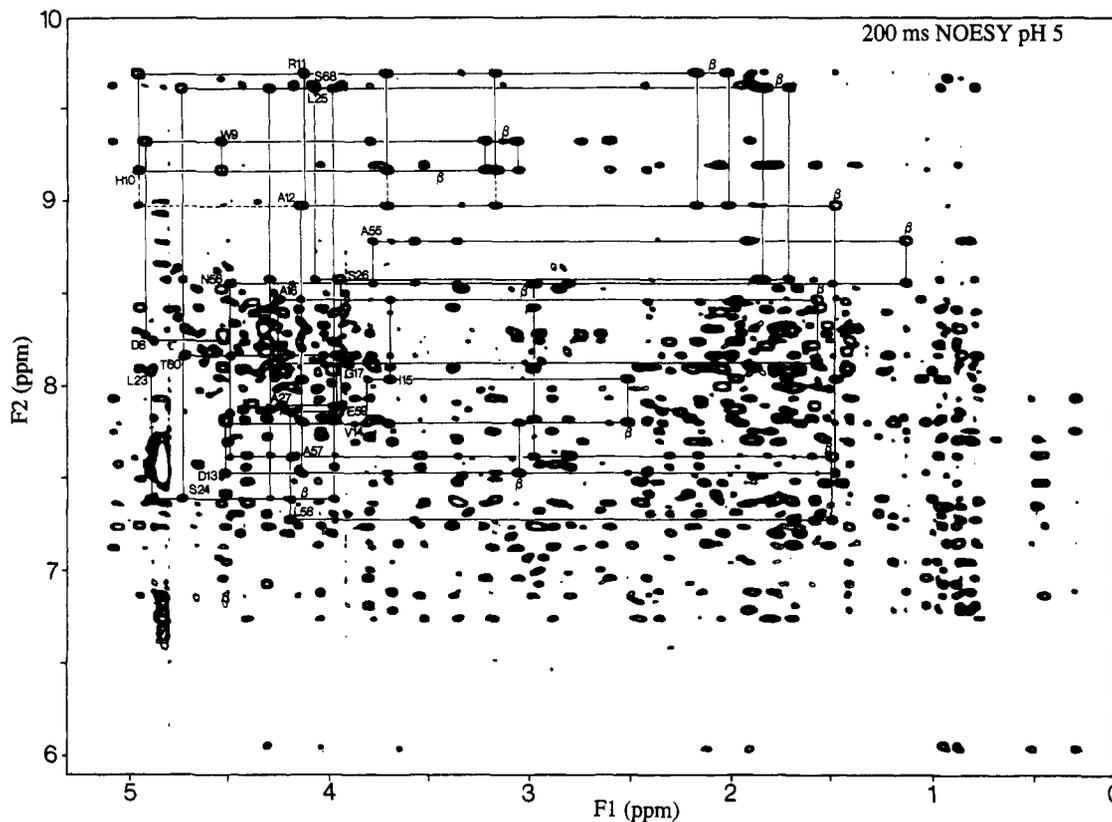
FIGURE 4: NH/aromatic(F_2 axis)–aliphatic(F_1 axis) region of the 200-ms NOESY spectrum in H_2O at pH 5.0. Stretches of $C^\alpha H(i)$–NH(i + 1) and $C^\beta H(i)$–NH(i + 1) connectivities extending over residues 8–17, 23–27, and 55–60 are indicated by continuous lines, while some longer range connections are marked by a dashed line.
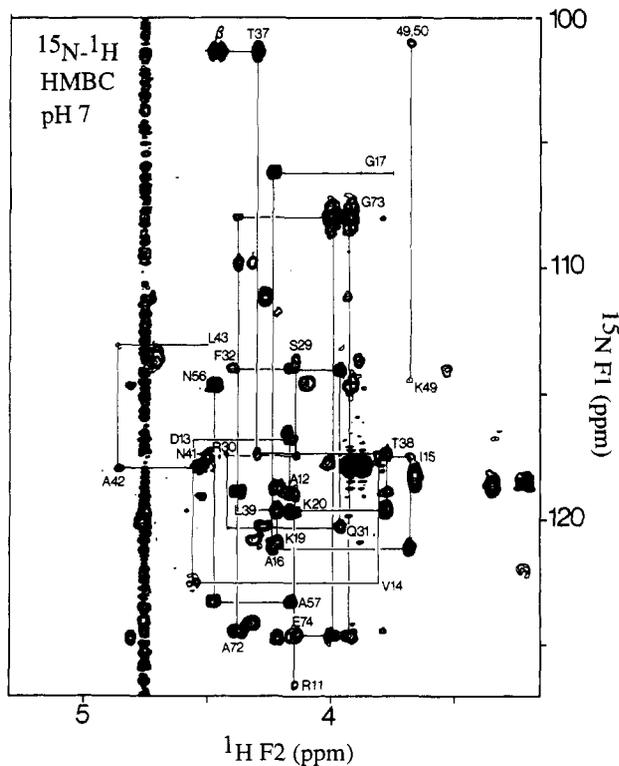

FIGURE 5: $^{15}N(F_1$ axis)–aliphatic(F_2 axis) region of the ^{15}N–^1H HMBC spectrum of ^{15}N-labeled Ner in D_2O at 27 °C and pH 7.0. Cross peaks arise from long range two- and three-bond correlations of the type $C^\alpha H(i)$–$^{15}N(i)$, $C^\alpha H(i - 1)$–$^{15}N(i)$, and $C^\beta H(i)$–$^{15}N(i)$. Labels are at the positions of intraresidue cross peaks. Sequential connectivities are indicated over residues 11–17, 19–20, 29–32, 37–39, 41–43, 49–50, 56–57, and 72–74.

shift in the same direction is also observed for the NH resonance of Asp-13. Thus, it could well be that the N-terminal

end of the first helix (or an adjacent turn) is more stable at higher pH values, reflected by the observed chemical shift changes. We found no evidence for stretches of β-strand or a β-sheet region in the Ner protein. We observed only two regions exhibiting strong consecutive $C^\alpha H(i)$–NH(i + 1) connectivities characteristic of an extended conformation. The most prominent is located at the N-terminus (residues 6–8), for which no other sequential NOEs were found. This, together with the absence of sequential NOEs between residues 1 and 6, suggests that the first eight amino acids do not form a regular secondary structure, but rather adopt a random coil conformation. The second stretch of medium to strong $C^\alpha H$-(i)–NH(i + 1) connectivities was found between residues 21 and 26, which appears to form an exposed loop connecting the first and second helices.

It may be of interest to compare the NMR-derived secondary structure with the secondary structure predictions of the Chou–Fasman (1978) or Garnier–Robson (Garnier et al., 1978) algorithms. The former predicts α-helix throughout the sequence up to the last 10 amino acids that have β-sheet propensity, interrupted by two turns centered around proline 36 and proline 48; the latter predicts helix up to position 23, β-sheet from position 23 to position 30, followed by a turn (residues 31–33), a helix from residue 39 to residue 59, a turn centered around proline 62, and no preference for the last 10 amino acids. Apart from the fact that a predominantly helical structure is predicted, the agreement is not very strong. Only the third and fourth helices with the adjacent turns are predicted reasonably well, while the remaining parts of the sequence differ in the two predictions as well as from the experimentally determined secondary structure.

With the secondary structure elements of Mu Ner in hand, it is of interest to go back and look again for homologies with other helix–turn–helix-containing DNA binding proteins. A comparison with the secondary structure elements found in
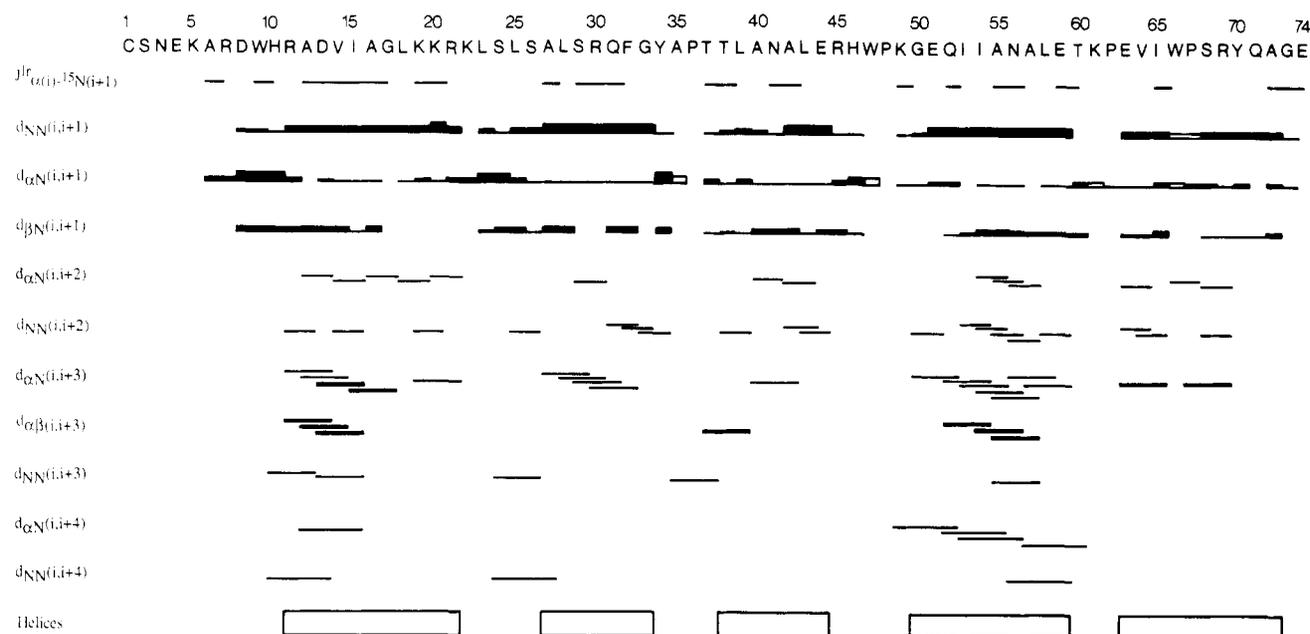
FIGURE 6: Amino acid sequence of the Ner protein with a summary of all three-bond $C^\alpha H(i)-{}^{15}N(i + 1)$ scalar connectivities as well as all short-range NOE connectivities involving the NH, $C^\alpha H$, and $C^\beta H$ protons. The $NH(i + 1)-C^\delta H(i)$ and $C^\alpha H(i)-C^\delta H(i + 1)$ NOEs involving the $C^\delta H$ protons of proline residues are represented by open bars along the line of the $NH(i)-NH(i + 1)$ and $C^\alpha H(i)-NH(i + 1)$ NOE connectivities, respectively.

the three-dimensional structure of the cro protein of λ (Anderson et al., 1981) shows that in this case only three helices comprising residues 7–13, 15–23, and 27–36 are found, with the second and third helices forming the helix–turn–helix motif. The rest of the cro structure is made up of three β-strands forming an antiparallel β-sheet. Therefore, despite the functional homology between λ cro and Mu Ner, no stringent structural homology is found. A comparison, however, with the secondary structure elements found in the crystal structure of the λ repressor headpiece (Pabo & Lewis, 1982; Jordan & Pabo, 1988) and 434 repressor headpiece (Anderson et al., 1987; Aggarwal et al., 1988), both of which are similar in size to Mu Ner, yields the interesting observation that these two protein domains also contain five α-helices and no β-structure, similar to our findings for the Ner protein. In addition, a recent report of the crystal structure of a protein–DNA complex formed by the cro protein of a different phage, namely, phage 434, shows that the 434 cro structure is made up of five helices and has a very similar structure to that of the 434 repressor headpiece (Wolberger et al., 1988). It may therefore well be that the polypeptide fold of Mu Ner is structurally homologous to that of the headpieces of the two phage repressor proteins and 434 cro. Since at the present stage we cannot ascertain an alignment based on the amino acid sequence and no information is available as to the spatial arrangement of the helices for the Ner Protein, we cannot answer the pertinent question of whether the Ner protein contains a helix–turn–helix motif as found in these other DNA binding proteins. This has to await a full structural characterization of the complete protein structure based on additional NOE data and in particular NOEs between residues far apart in the sequence, which are currently being analyzed in our laboratory.

SUPPLEMENTARY MATERIAL AVAILABLE

Two figures illustrating the $C^\alpha H(F_1$ axis)–aliphatic(F_2 axis) region of a HOHAHA spectrum in D_2O and the $NH(F_2$ axis)–aliphatic(F_1 axis) region of a NOESY spectrum in H_2O at pH 7 (4 pages). Ordering information is given on any current masthead page.

REFERENCES

Aggarwal, A. L., Rodgers, D. W., Drottar, M., Ptashne, M., & Harrison, S. C. (1988) *Science 242*, 899–907.

Allet, B., Payton, M., Mattaliano, R. J., Gronenborn, A. M., Clore, G. M., & Wingfield, P. T. (1988) *Gene 65*, 259–268.

Anderson, J. E., Ptashne, M., & Harrison, S. C. (1988) *Nature 326*, 846–852.

Anderson, W., Ohlendorf, D., Takeda, Y., & Matthews, B. (1981) *Nature 290*, 754–758.

Anderson, W., Takeda, Y., Ohlendorf, D., & Matthews, B. (1982) *J. Mol. Biol. 159*, 745–751.

Bax, A. (1989) *Methods Enzymol.* (in press).

Bax, A., & Marion, D. (1988) *J. Magn. Reson. 78*, 186–191.

Bax, A., Griffey, R. H., & Hawkins, B. L. (1983) *J. Am. Chem. Soc. 105*, 7188–7190.

Bax, A., Sklenar, V., Clore, G. M., & Gronenborn, A. M. (1987) *J. Am. Chem. Soc. 109*, 6511–6513.

Bax, A., Kay, L. E., Sparks, S. W., & Torchia, D. A. (1989) *J. Am. Chem. Soc. 111*, 408–409.

Billeter, M., Braun, W., & Wüthrich, K. (1982) *J. Mol. Biol. 155*, 321–345.

Braunschweiler, L., & Ernst, R. R. (1983) *J. Magn. Reson. 53*, 521–528.

Bystrov, V. F. (1976) *Prog. Nucl. Reson. Spectros. 10*, 41–82.

Chou, P. Y., & Fasman, C. D. (1978) *Adv. Enzymol. Relat. Areas Mol. Biol. 47*, 45–148.

Clore, G. M., Bax, A., Wingfield, P. T., & Gronenborn, A. M. (1988) *FEBS Lett. 238*, 17–21.

Davis, D. G., & Bax, A. (1985) *J. Am. Chem. Soc. 107*, 2821–2822.

Driscoll, P. C., Clore, G. M., Beress, L., & Gronenborn, A. M. (1989) *Biochemistry 28*, 2178–2187.

Garnier, J., Osguthrope, D. J., & Robson, B. (1978) *J. Mol. Biol. 120*, 97–120.

Glushka, J., & Cowburn, D. (1987) *J. Am. Chem. Soc. 109*, 7879–7881.

Goosen, N. (1984) Regulation of Transposition of Bacterio-

phage Mu, Ph.D. Thesis, State University of Leiden, The Netherlands.

Goosen, N., & van de Putte, P. (1984) *Gene 30*, 41–46.

Gronenborn, A. M., Bax, A., Wingfield, P. T., & Clore, G. M. (1989) *FEBS Lett. 243*, 93–98.

Jeener, J., Meier, B. H., Bachmann, P., & Ernst, R. R. (1979) *J. Chem. Phys. 71*, 4546–4533.

Jordan, S. R., & Pabo, C. O. (1988) *Science 242*, 893–899.

Macura, S., Huang, Y., Suter, D., & Ernst, R. R. (1981) *J. Magn. Reson. 43*, 259–281.

Marion, D., & Wüthrich, K. (1983) *Biochem. Biophys. Res. Commun. 113*, 967–974.

Marion, D., & Bax, A. (1988a) *J. Magn. Reson. 80*, 528–533.

Marion, D., & Bax, A. (1988b) *J. Magn. Reson. 79*, 352–356.

Mueller, L. (1979) *J. Am. Chem. Soc. 101*, 4481–4484.

Pabo, C., & Lewis, M. (1982) *Nature 298*, 443–447.

Pabo, C. O., & Sauer, R. T. (1984) *Annu. Rev. Biochem. 53*, 293–321.

Plateau, P., & Gueron, M. (1982) *J. Am. Chem. Soc. 104*, 7310–7311.

Redfield, A. G. (1983) *Chem. Phys. Lett. 96*, 537–540.

Redfield, A. G., & Kuntz, S. D. (1975) *J. Magn. Reson. 19*, 250–254.

Sklenar, V., & Bax, A. (1987) *J. Magn. Reson. 71*, 379–383.

Tolias, P. P., & DuBow, M. S. (1986) *Virology 148*, 293–311.

Van de Putte, P., Giphart-Gassler, M., Goosen, N., Goosen, T., & van Leerdam, E. (1988) *Cold Spring Harbor Symp. Quant. Biol. 45*, 347–353.

Van Leerdam, E., Karreman, C., & van de Putte, P. (1982) *Virology 123*, 19–28.

Wolberger, C., Dong, Y., Ptashne, M., & Harrison, S. C. (1988) *Nature 335*, 789–795.

Wüthrich, K. (1986) *NMR of Proteins and Nucleic Acids*, Wiley, New York.

Wüthrich, K., Billeter, M., & Braun, W. (1984) *J. Mol. Biol. 180*, 715–740.

Dynamics of Antarctic Fish Microtubules at Low Temperatures[†]

Richard H. Himes[‡] and H. William Detrich, III[*,§]

Department of Biochemistry, University of Kansas, Lawrence, Kansas 66045, and Department of Biology, Northeastern University, Boston, Massachusetts 02115

ABSTRACT: The tubulins of Antarctic fishes, purified from brain tissue and depleted of microtubule-associated proteins (MAPs), polymerized efficiently in vitro to yield microtubules at near-physiological and supraphysiological temperatures (5, 10, and 20 °C). The dynamics of the microtubules at these temperatures were examined through the use of labeled guanosine 5′-triphosphate (GTP) as a marker for the incorporation, retention, and loss of tubulin dimers. Following attainment of a steady state in microtubule mass at 20 °C, the rate of incorporation of [^{3}H]GTP (i.e., tubulin dimers) during pulses of constant duration decreased asymptotically toward a constant, nonzero value as the interval prior to label addition to the microtubule solution increased. Concomitant with the decreasing rate of label incorporation, the average length of the microtubules increased, and the number concentration of microtubules decreased. Thus, redistribution of microtubule lengths (probably via dynamic instability and/or microtubule annealing) appears to be responsible for the time-dependent decrease in the rate of tubulin uptake. When the microtubules had attained both a steady state in mass and a constant length distribution, linear incorporation of labeled tubulin dimers over time occurred at rates of 1.45 s^{-1} at 5 °C, 0.48 s^{-1} at 10 °C, and 0.18 s^{-1} at 20 °C. Thus, the microtubules displayed greater rates of subunit flux, or treadmilling, at lower, near-physiological temperatures. At each temperature, most of the incorporated label was retained by the microtubules during a subsequent chase with excess unlabeled GTP. In contrast, when microtubules were assembled de novo in the presence of [α-^{32}P]GTP at 5 °C and then exposed to a pulse of [^{3}H]GTP, the ^{32}P label was lost over time during a subsequent chase with unlabeled GTP, whereas the ^{3}H label was retained. Together, these results indicate that the microtubules of Antarctic fishes exhibit, at low temperatures, behaviors consistent both with subunit treadmilling and with dynamic instability and/or microtubule annealing.

Microtubules assembled in vitro are dynamic, not static, structures. Depending upon their protein composition, the total polymer concentration, and other solution conditions, the microtubules of warm-blooded animals may exhibit subunit "treadmilling" [the net, balanced addition and loss of tubulin subunits at opposite microtubule ends (Margolis & Wilson, 1978)], "dynamic instability" [the coexistence at constant polymer mass of subpopulations of rapidly shrinking and slowly growing microtubules that interconvert rarely (Mitchison & Kirschner, 1984)], and/or end-to-end "annealing" [the joining of segments of preformed microtubules to produce longer microtubules (Rothwell et al., 1986)]. Eukaryotic cells may exploit these phenomena to modulate the assembly and stability of their microtubules in processes such as mitosis or cellular morphogenesis (Kirschner, 1980; Kirschner & Mitchison, 1986; Rothwell et al., 1986). If these processes are important physiologically, then the "cold-stable" microtubules

   © 1989 American Chemical Society